

## TRANSIENT SPIRALS AS SUPERPOSED INSTABILITIES

J. A. SELLWOOD

Department of Physics and Astronomy, Rutgers University,  
136 Frelinghuysen Road, Piscataway, NJ 08854  
sellwood@physics.rutgers.edu

AND

R. G. CARLBERG

Department of Astronomy and Astrophysics, University of Toronto,  
Toronto, ON M5S 3H4, Canada  
carlberg@astro.utoronto.ca

*Revised version to appear in ApJ*

### ABSTRACT

We present evidence that recurrent spiral activity, long manifested in simulations of disk galaxies, results from the super-position of a few transient spiral modes. Each mode lasts between 5 and 10 rotations at its corotation radius where its amplitude is greatest. The scattering of stars as each wave decays takes place over narrow ranges of angular momentum, causing abrupt changes to the impedance of the disk to subsequent traveling waves. Partial reflections of waves at these newly created features, allows new standing-wave instabilities to appear that saturate and decay in their turn, scattering particles at new locations, creating a recurring cycle. The spiral activity causes the general level of random motion to rise, gradually decreasing the ability of the disk to support further activity unless the disk contains a dissipative gas component from which stars form on near-circular orbits. We also show that this interpretation is consistent with the behavior reported in other recent simulations with low mass-disks.

*Subject headings:* Galaxies — galaxies: kinematics and dynamics — galaxies: spiral — galaxies: structure — instabilities

### 1. INTRODUCTION

The origin of spiral patterns in galaxies still has no fully satisfactory dynamical explanation (see reviews by Binney & Tremaine 2008; Sellwood 2013a). Compelling observational evidence, both photometric (Schweizer 1976; Gnedin *et al.* 1995; Grosbøl *et al.* 2004; Zibetti *et al.* 2009) and kinematic (Visser 1978; Chemin *et al.* 2006; Shetty *et al.* 2007), indicates that spiral patterns are gravitationally driven density waves in the stellar disk. Kormendy & Norman (1979) and Kendall *et al.* (2011) found that the best developed, regular patterns are observed in interacting galaxies and perhaps also those with bars. While the behavior in these cases may not be entirely understood, at least the driving mechanism is clear.

The majority of disk galaxies with a significant gas component (*e.g.* Oort 1962) display less regular patterns, whose origin is not so easily accounted for. The spiral patterns may have some vague rotational symmetry, which is predominantly 2- or 3-fold (Davis *et al.* 2012, their Table 2), but it is usually far from perfect as arms bifurcate and/or fade with radius. The ubiquity of the phenomenon, taken together with the fact that simulations of isolated, unbarred, cool collisionless stellar disks (cited below) always manifest similar patterns, argues that there must be a mechanism for self-excitation, which is the question we address here.

No galaxy in our hierarchical universe is truly isolated, and infalling subhalos are predicted to bombard the outer halo of every galaxy (*e.g.* Boylan-Kolchin *et al.* 2010). Since tides can excite spiral responses, it is possible some patterns are excited by halo substructure (*e.g.* Dubinski *et al.* 2008). But the inner halos of galaxies, where fragile thin disks reside, are quite smooth (Gao *et al.* 2011)

and even large subhalos, such as that which hosted the Sagittarius dwarf galaxy (Belokurov *et al.* 2006), can be severely tidally disrupted before perturbing the disk (Purcell *et al.* 2011). We argue here that spiral patterns appear so readily as self-excited instabilities that disk responses to diffuse sub-halo perturbations probably give rise to a minority of spirals.

Continuously changing recurrent transient patterns have been reported over many years from simulations of isolated, unbarred disk galaxy models (*e.g.* Hockney & Brownrigg 1974; Sellwood & Carlberg 1984; Roškar *et al.* 2008) and no qualitatively different behavior has emerged as the numerical quality has improved. Claims of long-lived spiral modes have not proven to be reproducible (Sellwood 2011). Spiral activity fades over time as stellar random motions rise due to scattering by the fluctuating spiral patterns, but a reasonable amount of gas infall and dissipation can prolong spiral activity apparently indefinitely (*e.g.* Sellwood & Carlberg 1984; Carlberg & Freedman 1985; Toomre 1990), which is also consistent with modern galaxy formation simulations (*e.g.* Agertz *et al.* 2011).

Here, we finally address the issue that was left unexplained in Sellwood & Carlberg (1984, hereafter Paper I), namely the nature of the spirals that arise in such simulations. In a follow-up study to our original work (Sellwood 1989), we reported that the continuously changing patterns appeared to result from the superposition of a few longer-lived waves, each of which had well-defined frequencies and shapes and lasted for between five and ten full rotations of the pattern. These properties are consistent with them being modes, or standing waves, although they did not last indefinitely. Here we provide stronger evidence and propose a mechanism for this interpretation, using simulations of altogether higher quality than those

in our original study.

## 2. SIMULATIONS

Computational resources available at the time required that the simulations presented in Paper I employed typically just  $2 \times 10^4$  particles whose motion was confined to a plane. Here we continue to employ the same basic physical model, with a fraction of the total mass in a disk represented by particles, while the remaining central attraction comes from a rigid mass distribution, but we present results with greatly increased numbers of particles and also full three-dimensional (3D) motion.

We mimicked dissipation in some of our models in Paper I, but we do not attempt to do so here in order to focus on purely collisionless dynamics. All the models reported below therefore heat as a result of spiral activity (Carlberg & Sellwood 1985) until the disk becomes featureless after some number of rotations.

### 2.1. Mass Model

The radial surface density profile of the disk has the form we employed in Paper I

$$\Sigma(R) = 1.563 \frac{M}{a^2} \left(1 + \frac{20R}{a}\right)^{-3/4} \left(1 + \frac{R}{5a}\right)^{-2}, \quad (1)$$

and a circular velocity curve

$$V(R) = 1.956V_0 \frac{R}{a} \left(1 + \frac{2R}{a}\right)^{-7/8} \left(1 + \frac{R}{5a}\right)^{-5/8}, \quad (2)$$

where  $a$  is a length scale, and  $M$  a mass unit; thus the velocity unit and dynamical time are, respectively,  $V_0 = (GM/a)^{1/2}$  and  $\tau_0 = (a^3/GM)^{1/2}$ .<sup>1</sup> Expressions (1) and (2) are not perfectly self-consistent, but a numerical solution with softened gravity for the central attraction of the surface density (1) gives a rotation curve that is quite well fitted by the function  $V(R)$  in eq. (2). In Paper I, we devised this unconventional model to meet two objectives: (1) to produce a rotation curve that superficially resembled that of a large Sc galaxy, and (2) to yield a model that developed spirals all over the disk, since we had found that quasi-uniform rotation in the inner disk prevented spirals from developing there.

We employ this model again in the present paper for comparison to our earlier work. Although the disk mass profile is not the usual exponential, it is not unreasonable; our conclusions seem quite general, and should hold in any plausible model of a differentially rotating disk. We continue to employ a rigid halo principally because our focus is on spiral dynamics. While it remains to be demonstrated explicitly, we believe that a responsive halo would have very little affect on the spiral evolution; bars can lose angular momentum to halos through resonant interactions (Tremaine & Weinberg 1984), but spirals have both lower amplitude and shorter lifetimes than do bars and, hence, couple much more weakly to a halo. We showed in Paper I that gas was important to prolong the lifetimes of the patterns, but omit this aspect also. In summary, the simplified experiments presented here have allowed us to develop an understanding of the driving mechanism for

<sup>1</sup> The bizarre proportionality constants in eqs. (1) and (2) are needed to reconcile the units used in Paper I with those used here.

spirals in the stellar disk only, which seems to be the key part according to the observational evidence reviewed in the introduction.

We use a cubic function to taper the surface density smoothly to zero over the range  $6.5a < R < 7.5a$ , leaving a total disk mass of  $\simeq 3.4M$  with the half-mass radius being  $R_e \simeq 2.75a$ . The circular speed has a broad maximum of  $V \simeq 0.8V_0$  around  $R \sim 3a$ , and a rotation period at  $R = R_e$  is  $\sim 20$  dynamical times. Since the scaling to physical units is arbitrary, we here set  $G = M = a = 1$ ; one possible scaling is to choose  $a = 3$  kpc and  $\tau_0 = 10$  Myr, leading to  $V_0 \simeq 293$  km s<sup>-1</sup> and  $M \simeq 6.0 \times 10^{10} M_\odot$ .

In practice, we use a disk with a fractional surface density  $f$ , of that given in eq. (1), while the contribution from the rigid matter gives  $V^2(1-f)/r$  to the central attraction, with  $V$  given by eq. (2). In Paper I, our simulations started with  $f = 0.3$  to inhibit vigorous bar-forming instabilities in the disk.

We start all simulations with  $Q = 1$  at all radii, where

$$Q(R) = \frac{\sigma_R}{\sigma_{R,\text{crit}}}, \quad \text{with} \quad \sigma_{R,\text{crit}} = \frac{3.36Gf\Sigma(R)}{\kappa(R)}. \quad (3)$$

(Toomre 1964). Here  $\sigma_R(R)$  is the local radial velocity dispersion of particles in the disk and  $\kappa$  is the usual Lindblad epicycle frequency. We set the azimuthal dispersion and mean orbital speed using the Jeans equations in the epicycle approximation. In 3D models, we distribute particles in  $z$  using a Gaussian of width  $z_0 = 0.05$ , and construct vertical equilibrium by solving the 1D Jeans equation in the vertical restoring force computed from the particles. Since the disk mass is low, this procedure yields models that are close enough to equilibrium that no initial relaxation is required.

We generally compute the evolution for  $500\tau_0$ . We use a basic time step  $\delta t = 0.05\tau_0$ , and the time step is increased by successive factors of two in three annular zones of greater radii. In 2D, we adopt Plummer softening with softening length  $\epsilon = 0.05$  and a grid with 128 radial spokes and 96 logarithmically spaced rings. In 3D models, we employ a cubic spline law (Monaghan & Lattanzio 1985) with  $\epsilon = 0.04$  and grid of  $96 \times 128 \times 125$  mesh points.

Our numerical techniques are described in full detail in <http://www.physics.rutgers.edu/~sellwood/code/manual.pdf>.

### 2.2. Two-dimensional Models

We first present a series of simulations with  $f = 0.3$  and other physical properties exactly as we used in our first model from Paper I— but which have increasing numbers of particles. All the models manifested spiral activity resembling that in our earlier paper.

Initial spiral activity is seeded by shot noise, which has an amplitude that scales as  $N^{-1/2}$ . While chance leading wave components in the spectrum of shot noise give rise to responses that are swing-amplified by a substantial factor (Goldreich & Lynden-Bell 1965; Toomre 1981), we showed in Paper I that the expected noise level was below the measured leading signal even with  $N = 2 \times 10^4$ , and is correspondingly lower still in the present experiments with much greater numbers of particles. Spiral activity at the amplitude we observe must be boosted either by feedback creating unstable modes or by non-linear effects or both, as we discuss in §3.

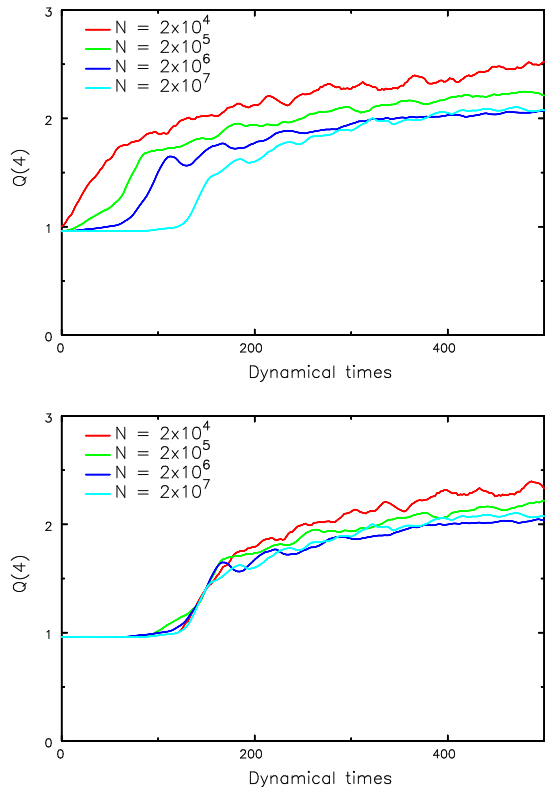


FIG. 1.— Time evolution of  $Q$  at  $R = 4$  in four simulations with increasing numbers of particles, still confined to move in a plane. In the lower panel, the curves have been shifted horizontally so that all pass through  $Q = 1.4$  at the same moment, which required larger time shifts in the experiments with smaller  $N$ . Note that a rotation period at the half-mass radius is 20 dynamical times.

Fig. 1 shows the time evolution of  $Q$  at a radius of  $R = 4$  measured from the simulations. Spiral activity heated all the models, but as we employed more particles, the spirals took increasingly long to develop. To compensate for this delay, which we account for in §3, we slide the curves from the smaller  $N$  models to the right in the lower panel so that they all coincide as  $Q$  rises through 1.4, which reveals that the  $N = 2 \times 10^4$  model, as used in Paper I, heated a little more rapidly and to a slightly higher value of  $Q$  than did the larger  $N$  models.

However, the heating rates are all very similar once spiral activity gets going, indicating that rapid heating is not caused by two-body relaxation, as some authors (*e.g.* Fujii *et al.* 2011) have suggested. We offer four additional reasons to reject their conjecture. First, we noted in Paper I that heating was much less rapid in the inner disk of a Kuzmin-Toomre model, where shear is weak and spiral activity was insignificant, indicating that heating was caused by the spirals and not by relaxation. Second, the same code has been used with similar particle numbers to reproduce the normal modes expected from stability analyses of smooth stellar fluids (Sellwood & Athanassoula 1986) which would be impossible if relaxation were rapid. Third, the code reproduced the behavior in a solution of the collisionless Boltzmann equation (Inagaki *et al.* 1984). Finally, relaxation in 2D systems differs fundamentally from that in 3D (Rybicki 1972; Sellwood 2013b), and is readily controlled by force softening. The slower heat-

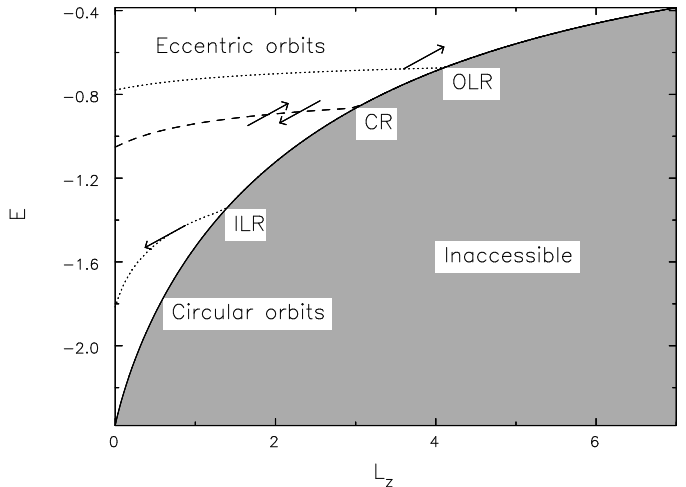


FIG. 2.— Lindblad diagram showing specific energy,  $E$ , as a function of angular momentum,  $L_z$ , for particles in our Sc model. Eccentric orbits lie in the region above the solid curve, which is for circular orbits. The dashed and dotted curves show the loci of respectively corotation and the two Lindblad resonances for an  $m = 3$  disturbance with  $\Omega_p = 0.07$ . The arrows mark possible scattering vectors at the three principal resonances.

ing in the experiments by Fujii *et al.* (2011) and others is accounted for in §4.3.

See §3 for an explanation of the origin of spirals and §4 for further discussion of related work by other authors.

### 2.3. Spiral Heating

In all cases, the model heated to  $Q \gtrsim 2$  in a few disk rotations, and the increased random motion caused spiral activity to fade, as reported in Paper I, and by others, in models without cooling. Because the dynamical time scale is shorter near the center, the inner disk heated more rapidly than the outer.

Scattering at the Lindblad resonances causes an irreversible increase in the level of random motion of the scattered particles (Carlberg & Sellwood 1985). Since Jacobi’s integral,  $I_J = E - \Omega_p L_z$ , is a conserved quantity in a non-axisymmetric potential that rotates steadily at rate  $\Omega_p$  (Binney & Tremaine 2008), changes of angular momentum  $\Delta L_z$  and specific energy are related as  $\Delta E = \Omega_p \Delta L_z$ . Thus stars are scattered along trajectories of fixed slope  $\Omega_p$  in the Lindblad diagram, shown in Fig. 2, and lasting changes occur only at resonances (Lynden-Bell & Kalnajs 1972). Note that the scattering vectors at the Lindblad resonances (dotted curves) are angled away from the slope of the circular orbit curve and scattered particles therefore gain energy of non-circular motion. Random motions rise everywhere because the simulations manifest multiple patterns with resonances distributed widely over the disk (§2.5).

In Paper I we demonstrated that a modest rate of addition of new particles on near-circular orbits, in a crude attempt to mimic accretion of cold gas that was immediately converted to star particles, was sufficient in this model to maintain spiral activity “indefinitely.” Spiral activity has also been shown to persist in simulations that employ other methods of cooling (*e.g.* Carlberg & Freedman 1985; Toomre 1990; Roškar *et al.* 2008; Agertz *et al.*

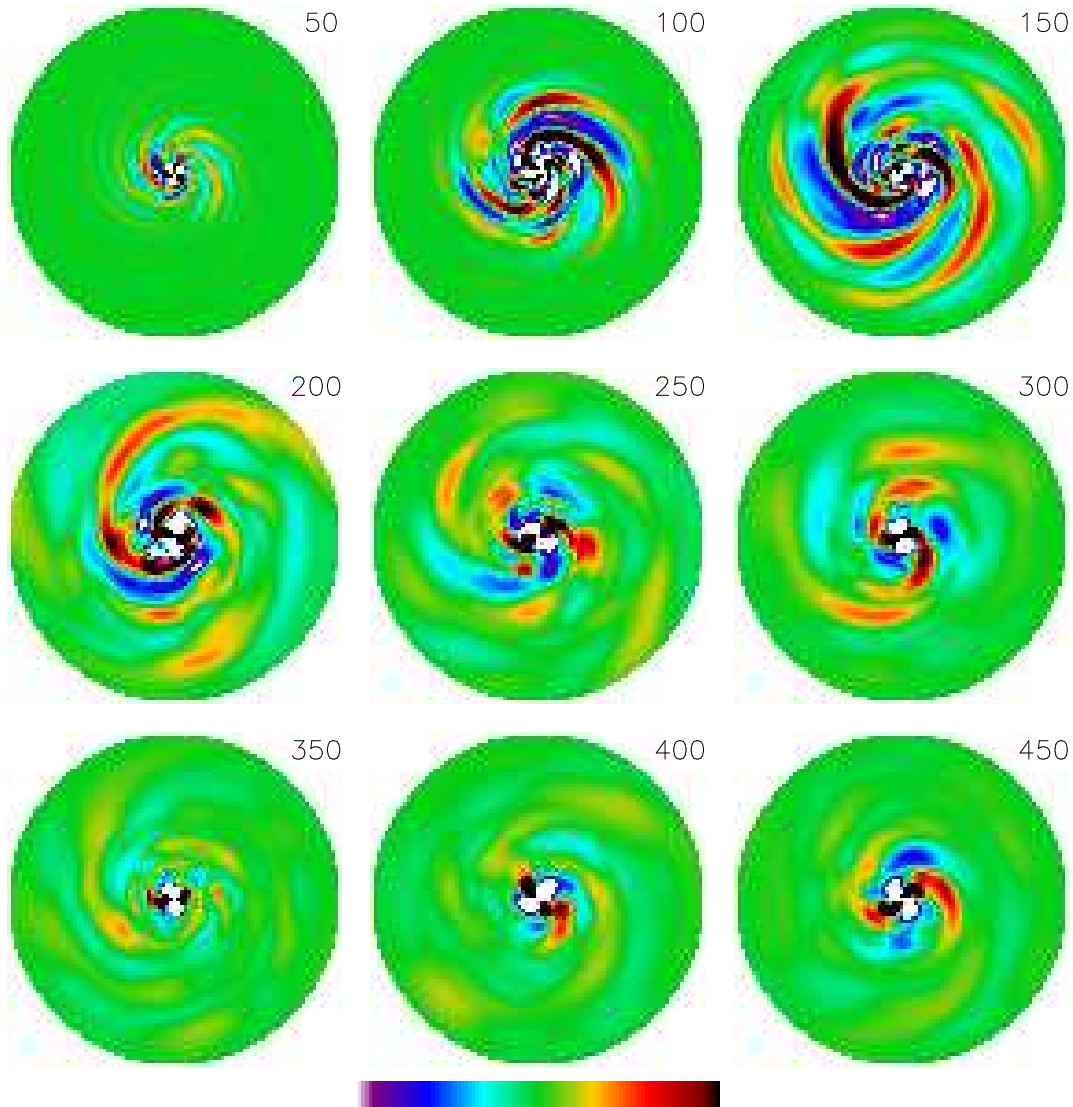


FIG. 3.— Surface density of particles in the  $N = 2 \times 10^8$  simulation at the times indicated. The color scale, which ranges over  $\pm 0.5$ , indicates the density relative to the mean at each radius; values outside this range are black or white. The radius of each circle is 8 disk scales. Notice that the spirals develop quite rapidly in the center, then spread outward before fading more slowly as the disk heats, while a small bar develops in the center.

2011). The persistence of spiral activity in cooled simulations provides an attractive explanation for the strong correspondence between the presence of spirals and gas in real galaxies (Oort 1962).

#### 2.4. 3D models

We next present simulations of the same mass models that allow full 3D motion for the disk particles. In addition, these models have  $f = 0.4$ , making the disk slightly more massive.

Employing  $N = 2 \times 10^4$  particles, while almost enough in 2D, is woefully inadequate once 3D motion is allowed, since the disk thickens excessively due to 2-body relaxation (Sellwood 2013b). We therefore present results from experiments with  $2 \times 10^5 \leq N \leq 2 \times 10^8$ .

Fig. 3 shows the perturbed surface density at a few times in the simulation with  $N = 2 \times 10^8$ , showing that the evolution resembles that of the uncooled model in Paper

I, even though the particle number was increased by four orders of magnitude and 3D motion is allowed. Fig. 4 shows the time evolution of  $Q(4)$  in these 3D models for which there is again a mild  $N$ -dependence. Once again, the onset of heating is more delayed as  $N$  rises because spiral activity takes longer to get going.

#### 2.5. Power Spectra

We use Fourier transforms to compute the gravitational field from the distribution of particles assigned to our polar grid at every step. We save the vertically integrated azimuthal Fourier coefficients of this mass distribution at each grid radius at regular intervals, typically 40 time steps, or  $\Delta t = 2$ . Fourier transformation in time of these coefficients yields the power as a function of frequency, for each sectoral harmonic,  $m$ , and radius  $R$ . The duration of the simulations is long enough, and the data saved at sufficiently frequent intervals, that we can subdivide the

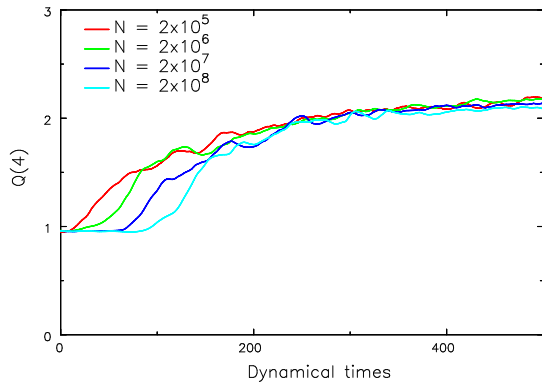


FIG. 4.— Time evolution of Toomre’s  $Q$  at  $R = 4$  in simulations in which 3D motion is allowed and  $f = 0.4$ . The four curves show results with different numbers of particles.

time range in order to compare the spectra from different periods of evolution.

The top (bottom) rows of Fig. 5 present power spectra for three sectoral harmonics from the first (second) half of the evolution of our 3D model with  $N = 2 \times 10^6$ . The contours are of power as functions of radius and frequency, the solid curve shows  $m\Omega_c$  and the dashed curves  $m\Omega_c \pm \kappa$ , where  $\Omega_c(R)$  is the angular frequency of circular motion and  $\kappa(R)$  is the Lindblad epicyclic frequency. Each horizontal ridge indicates a coherent density wave of frequency  $m\Omega_p$ , where  $\Omega_p$  is the pattern speed, that persisted for some time and extended over a range of radii. Plots from our larger  $N$  simulations are remarkably similar, although the precise frequencies of the ridges differ.

The ridges typically have the largest amplitudes near corotation and generally extend roughly as far as the Lindblad resonances, as expected from the locally derived dispersion relation for spiral waves (Binney & Tremaine 2008). In some cases, the wave outside corotation (CR) is very weak. Note that the high-frequency features near the center in the right panels ( $m = 4$ ) have twice the frequencies of the stronger inner features at  $m = 2$  (left panels), and are therefore not independent.

In the early part of the evolution, these coherent waves are strongest in the inner disk, but activity spreads outward over time, while it weakens in the inner disk, which is heated more rapidly as a result of the spiral activity. Movies of the time evolution of the power spectra from all our models reveal that each density ridge typically lasts for between 5 and 10 rotations at its corotation radius.

For each frequency in Fig. 5, the temporal Fourier transform yields the amplitude and phase of the wave at the initial moment. From this information, we can draw the shapes of the waves that give rise to the ridges in the power spectra. Fig. 6 shows the projected shapes of six waves that were marked with green horizontal lines in Fig. 5, with the corotation and Lindblad resonance radii for each drawn by solid and dotted circles, respectively. The wave in panel (a) is probably a bar mode, while each of the others has a trailing spiral form with peak amplitude near corotation; most have a more tightly wrapped feature near the inner Lindblad resonance (ILR).

## 2.6. Quiet Starts

The above results were obtained from simulations in which the initial azimuths of the particles were selected at random, causing the initial behavior to be driven by the shot noise from the random positions of the particles. We have also run several separate 2D quiet start simulations in order to identify instabilities of the *smooth* initial disk.

A quiet start (temporarily) suppresses activity excited by particle noise, since particles are initially spaced evenly around rings and disturbance forces are restricted to a single sectoral harmonic  $m$ . Provided the number of particles on each ring is  $> 2m + 1$ , forces from the ring are those of a mildly distorted uniform ring, allowing disturbances to grow by many  $e$ -folds before they saturate. Fitting the evolution of the amplitude and phase of the density variation in the linear regime yields the pattern speed and growth rate of dominant unstable mode(s) at each  $m$ ; see Sellwood & Athanassoula (1986) for a full description of the technique.

With  $m = 2$  only, we found a very slowly growing mode with  $\omega \simeq 0.71 + 0.03i$ ; the higher pattern speed of the bar mode in the noisy start model (Figures 5 and 6a) is probably seeded by shot noise. As the growing mode had an open bisymmetric spiral form with no ILR, it qualifies as a bar-forming cavity mode of the kind described in §3.1; the growth rate is low because the disk is sub-maximal. Because it grew so slowly, it did not produce a visible bar until  $t \simeq 480$  in the quiet start run. We found a much fiercer instability when forces were restricted to  $m = 3$  only: the measured frequency was  $\omega \approx 2.1 + 0.13i$ . This appeared to be another cavity-type mode, since its rotation rate is high enough to avoid an ILR. But even this fierce mode is outgrown, in noisy start simulations, by other features at larger radii as shown in the top middle panel of Fig. 5. There were no credible linear modes with  $m = 4$  only.

Note that we did not find any evidence for outer edge modes (Toomre 1981; Papaloizou & Lin 1989) in any of these quiet start simulations, although it is possible that one could be present at each  $m$ . Our tapered edge would cause any instability to grow too slowly to be detected and, if present, a mild instability would not affect the inner disk because the orbit time-scale is so much longer near the disk edge ( $R_{\max} = 7.5$ ).

## 3. NATURE OF THE WAVES

With the principal exception of the mode in Fig. 6(a) that gives rise to a small, persistent bar, we contend that almost all the ridges in the power spectra resulted from *transient spiral modes* of the form shown in the other panels of Fig. 6. Here we explain this interpretation more fully, and provide supporting evidence.

### 3.1. Swing-amplified Modes

The famous transient spiral presented by Toomre (1981, his Fig. 8), reproduced as Fig. 6.19 in Binney & Tremaine (2008), illustrates swing-amplification of a *wave packet*. The evolution is not that of a mode because the wave neither maintains a fixed shape nor grows indefinitely. Instead it is a *response* to a particularly provoking initial disturbance.

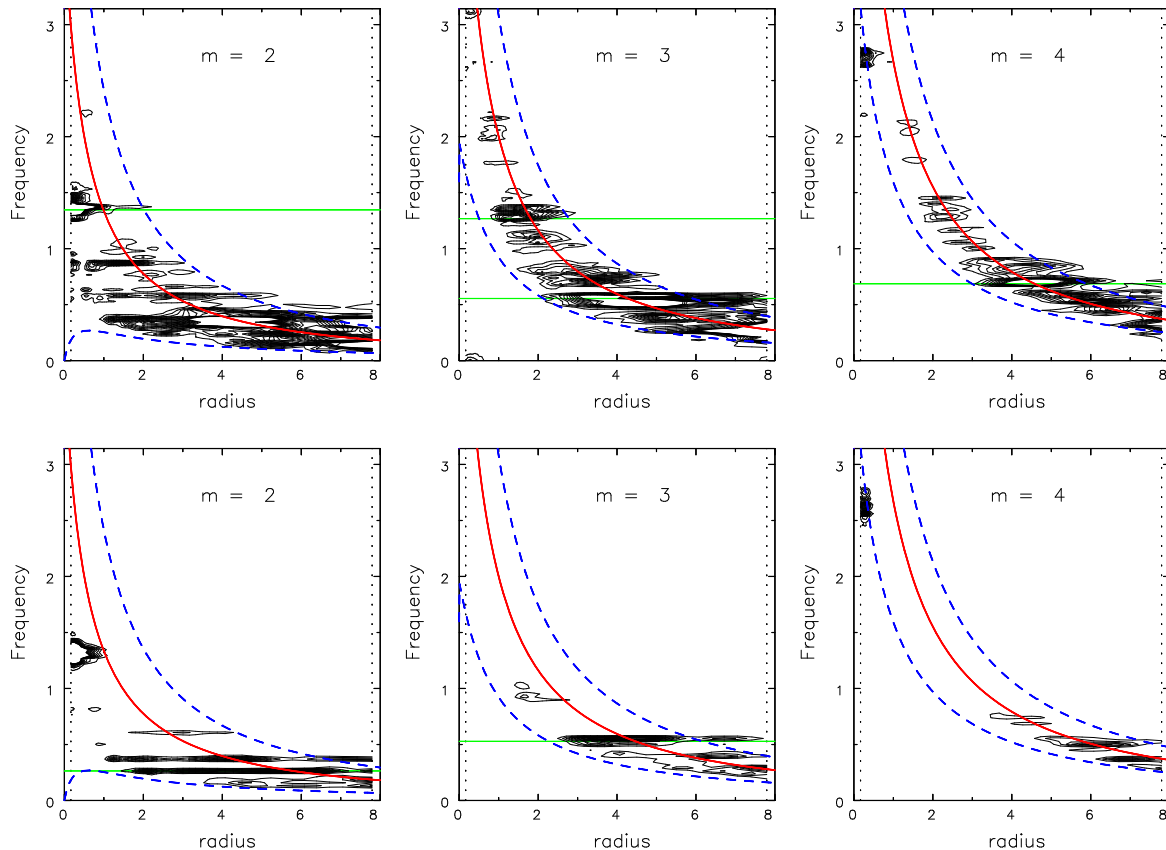


FIG. 5.— Contours of power as functions of radius and frequency for different sectoral harmonics  $m$  in our 3D model. The top row is for the first half of the evolution,  $22 \leq t \leq 260$ , the bottom row shows the second half  $262 \leq t \leq 500$ . In each panel, the solid (red) curve marks  $m\Omega_c$  and the dashed (blue) curves  $m\Omega_c \pm \kappa$ . Each horizontal stripe indicates a coherent wave with a well-defined angular frequency,  $m\Omega_p$ , over the time interval. The green horizontal lines mark the frequencies of the waves illustrated in Fig. 6.

After this transient swings from leading to trailing, accompanied by strong amplification, the spiral wave travels radially away from corotation at the group velocity (Toomre 1969),<sup>2</sup> advecting wave action, or angular momentum, across the disk. In a stellar disk with smoothly varying surface density and random motion, as was adopted for this calculation by Toomre, the wave propagates without significant losses as far as the Lindblad resonances, which are the only locations where the wave action can be absorbed by collisionless particles (Lynden-Bell & Kalnajs 1972; Mark 1974).

Modes, on the other hand, are standing waves between two reflecting ends, as is familiar from guitar-strings and organ pipes. If the in-going trailing wave can reflect off some feature, or the center, it becomes a leading wave with a group velocity directed back toward corotation. The outgoing leading wave incident on corotation is “super-reflected,” or swing-amplified, allowing a closed cycle with amplification. A growing mode is a continuous wavetrain that propagates around this cycle. As usual, only the frequencies for which the phase closes can give rise to standing waves.

<sup>2</sup> Strictly this is the direction of wave propagation on the short-wave branch of the dispersion relation only (Lin & Shu 1966; Binney & Tremaine 2008; Sellwood 2013a); the group velocity is in the opposite direction on the long-wave branch. However, the long-wave branch probably does not exist except in disks of very low mass (see the Appendix of Lynden-Bell & Kalnajs 1972).

Modes of this type are termed cavity modes. Reflection off the center is the mechanism for the bar-forming instability proposed by Toomre (1981). Here we suggest that reflections can also occur where previous disturbances have created features by resonant scattering in an initially smooth disk.<sup>3</sup>

### 3.2. Impedance changes

Wave particle interactions at Lindblad resonances scatter particles to more eccentric orbits and different angular momenta (Fig. 2). It is significant, as noted by Sellwood (2012) for  $m = 2$  waves in the Mestel disk, that scattering at the ILR is in a direction in the  $(L_z, E)$  plane that is almost along the locus of the ILR, and therefore each scattered particle stays on resonance causing large changes to its orbit from even quite mild spiral patterns. Furthermore, the ILR is localized so that only a small fraction of the particles are affected by it. This important feature of ILR scattering is quite general (Fig. 2 is drawn for an  $m = 3$  wave in our Sc model), and contrasts with the behavior at the OLR where small changes are shared by many particles that are each quickly scattered off resonance.

<sup>3</sup> Mark (1977) also proposed a feedback loop through reflection of waves off a feature in the inner part of a low-mass disk, but the  $Q$ -barrier he invoked caused more of a refraction of trailing waves from the short- to the long-wave branch of the dispersion relation.

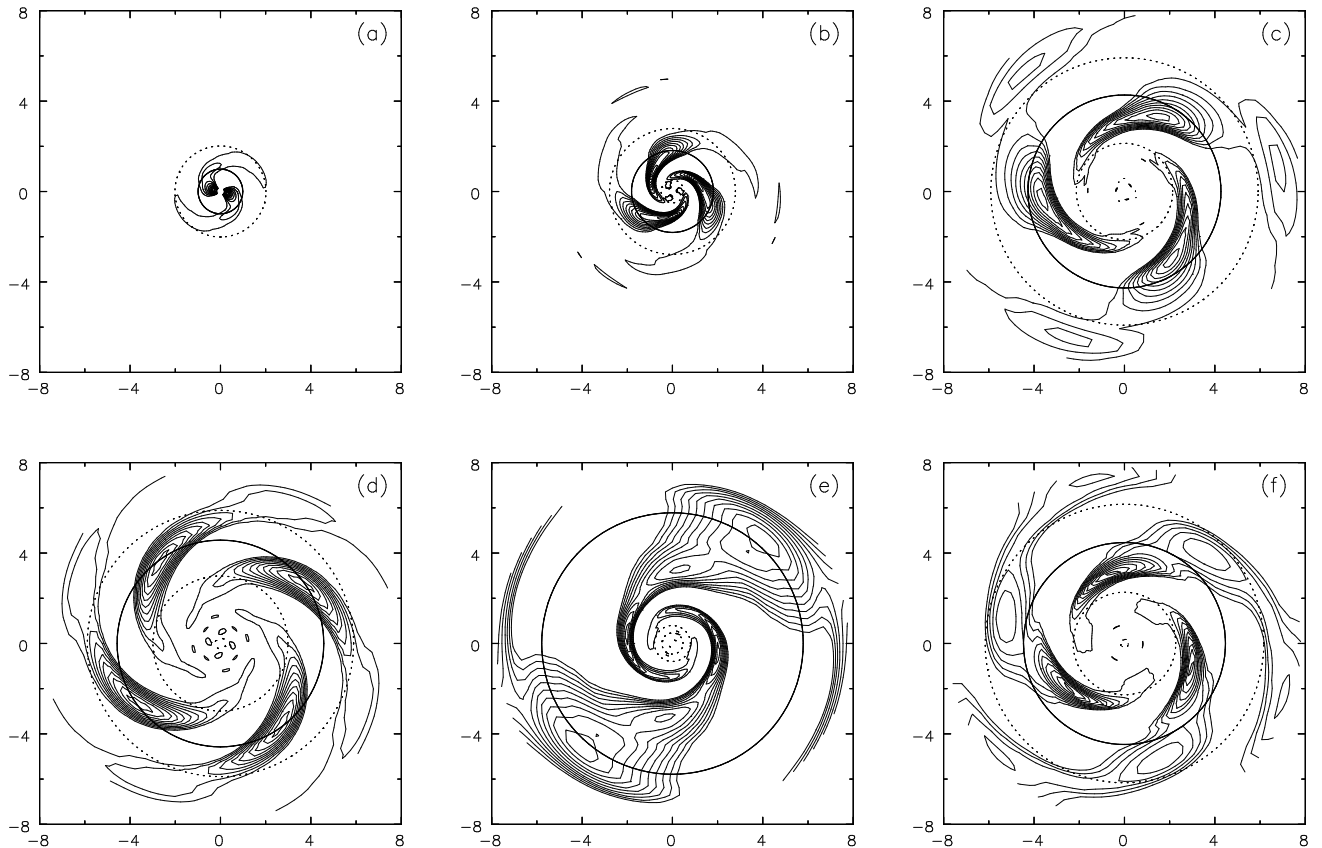


FIG. 6.— Projected shapes of the six long-lived waves marked with green lines in Fig. 5. Contours are of positive overdensity only and the solid circle marks corotation, while the dotted circles mark the Lindblad resonances. Panels (a) through (d) are from the first half of the evolution while (e) and (f) are from the later part.

The particles scattered at an ILR of one disturbance have increased radial excursions over a highly localized range of angular momenta. (We show this to be the case in our models in Fig. 8 below.) The effect of this locally increased random motion is that part of the disk will respond less cooperatively to subsequent waves as they travel across the disk, with important consequences. It is the abrupt change to the density of particles in action space that matters for spiral dynamics, which is not blurred by the increased epicyclic excursions.

Toomre (1969) applied the group velocity of a wave packet

$$v_g = \frac{\partial \omega}{\partial k}, \quad (4)$$

to spiral waves, for which  $\omega \equiv m\Omega_p$  and  $k$  are the pattern speed and radial wavenumber of the wave, respectively. The radial speed at which angular momentum is advected,  $v_g$  can be computed from the dispersion relation for spiral waves in a stellar disk, which is (in the WKB approximation)

$$(\omega - m\Omega)^2 = \kappa^2 - 2\pi G\Sigma\mathcal{F}(s, \chi)|k|, \quad (5)$$

(Lin & Shu 1966; Binney & Tremaine 2008; Sellwood 2013a). Here,  $\Omega$  and  $\kappa$  are the usual circular and epicycle frequencies in the axisymmetric potential, while  $\mathcal{F}(s, \chi)$  is the factor by which the responsiveness of the disk to the spiral potential is reduced compared with that were the disk to have no random motion. It depends on two properties of the

stellar distribution: the ratio of the forcing frequency experienced by a star to its natural frequency,  $s \equiv |\omega - m\Omega|/\kappa$ , and  $\chi \equiv \langle v_R^2 \rangle k^2 / \kappa^2$ , which is the square of the ratio of the typical sizes of the stellar epicycles ( $\propto \langle v_R^2 \rangle^{1/2} / \kappa$ ) to the wavelength of the wave ( $\propto |k|^{-1}$ ). When  $\chi$  is large,  $\mathcal{F} \ll 1$  because the unforced epicyclic amplitude of most stars is larger than the radial wavelength of the disturbance, and the weak supporting response arises mainly from the small fraction of stars near the center of the velocity distribution.

In our situation, there is an abrupt change to the sizes of the epicycles of stars that causes a corresponding abrupt change to  $\mathcal{F}$ . To understand how this affects the transmission of a spiral wave, it is useful to introduce the concept of impedance, familiar from electrical circuits or, more usefully, acoustic waves (see *e.g.* French 1971). The impedance in a stretched string, for example, is defined as  $Z = F_y/v_y = (T\mu)^{1/2}$ , where  $F_y$  and  $v_y$  are, respectively, the restoring force and displacement velocity in the vibration normal the  $x$ -direction of the equilibrium string,  $T$  is the tension and  $\mu$  the mass per unit length. When two strings with differing  $\mu$  are joined, the difference of impedance determines the reflection and transmission of waves across the join. For example, a wave in a heavy string is perfectly reflected at a join to a massless string.

Returning to spiral waves, the displacement velocity for

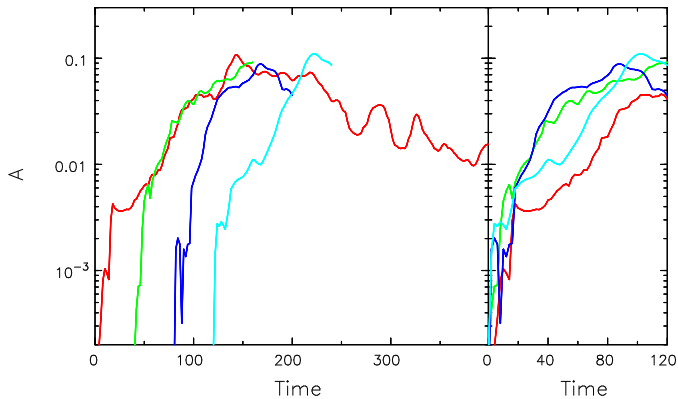


FIG. 7.— Amplitude evolution of the  $m = 3$ ,  $45^\circ$  trailing logarithmic spiral transform of the particle distribution in experiments with  $N = 2 \times 10^8$  particles. The red curve shows the evolution in the model used in Fig. 4, while the green, blue, and cyan curves show the behavior when the particles from that model have their azimuthal coordinates randomized after two, four, and six disk rotations, respectively. The right panel shows the same lines shifted to a common start time.

spiral waves in the local approximation is

$$\bar{v}_{Ra} = -\frac{\omega - m\Omega}{\kappa^2 - (\omega - m\Omega)^2} k\Phi_a \mathcal{F} \quad (6)$$

(Binney & Tremaine 2008, eq. 6.58), the impedance, therefore, is  $Z = k\Phi_a/\bar{v}_{Ra} \propto \mathcal{F}^{-1}$ , with the frequency factor dependent only on the properties of the axisymmetric potential and the pattern speed of the spiral. Thus, when a spiral wave traveling across a disk encounters an abrupt change to  $\mathcal{F}$ , it will be partly reflected and partly transmitted. In particular, a large decrease in  $\mathcal{F}$ , previously created by resonance scattering from an earlier wave, will be highly reflective.

### 3.3. Emergence from Noise

Sellwood (2012) studied the emergence of true instabilities from noise in highly restricted simulations of the half-mass Mestel disk with differing numbers of particles; motion was confined to a plane and perturbing forces arose from a single sectoral harmonic. He reported that changes caused by ILR scattering by earlier disturbances led to enhanced activity in the disk, presumably because the impedance change caused partial reflection of later incoming trailing waves. He found that the level of spiral activity exponentiated rather slowly until the reflections became strong enough to trigger an unstable global spiral mode with a much higher growth rate.

Our present simulations are slightly more general than those of Sellwood (2012), because they allow 3D motion and include multiple sectoral harmonics in the determination of the forces from the particles. However, we suggest that the recurrent cycle of modes also develops here because of impedance changes caused by resonance scattering in the inner disk.

In our large- $N$  experiments, swing-amplification of the initial low-amplitude shot noise created mild in-going spiral responses that are fully absorbed at the ILR causing important, though small, localized changes to the impedance of the disk. Subsequent responses to noise were partially reflected at these features, and the partial feedback boosted

later activity to a somewhat higher amplitude. As found by Sellwood (2012), several cycles of scattering by swing-amplified responses to shot noise were required before the impedance changes wrought by the absorption of these transient wave packets could give rise to reflections that were sufficiently strong to trigger instabilities. Hence, the increasing delay to the start of visible spiral activity and disk heating reported in Figs. 1 and 4.

Fig. 7 presents further evidence in support of this picture. Each curve shows the amplitude of the  $m = 3$ ,  $\cot \alpha = 1$  component of the transform

$$A(m, \alpha, t) = \frac{1}{N} \sum_{j=1}^N \exp[im(\phi_j + \cot \alpha \ln R_j)], \quad (7)$$

where  $(R_j, \phi_j)$  are the cylindrical polar coordinates of the  $j$ -th particle at time  $t$ , and  $\alpha$  is the pitch-angle of an  $m$ -arm logarithmic spiral, with positive values for trailing spirals. We have smoothed the curves in time using a running average of 10 consecutive values.

The red curve in Fig. 7 shows the time evolution of the amplitude,  $|A|$ , in our largest simulation ( $N = 2 \times 10^8$  particles). The other lines show the amplitude evolution in three further experiments, each derived from that used for the red line by restarting from randomized coordinates of all the particles after two, four and six rotations. We merely rotated the radius vector to each particle through a random angle, while preserving the radius,  $R$ , and the polar velocity components  $(v_R, v_\phi)$ . This procedure clearly destroyed all non-axisymmetric structure at that moment, and reduced the amplitude back to the shot noise level, while leaving the other parts of the phase space structure intact. It is clear that the green and blue curves rise more quickly than does the red, indicating that the models scrambled after two and four rotations possess more vigorous instabilities than did the original.

In the cases of the models restarted at  $t = 40$  and at  $t = 80$ , shown by the blue and green curves, we find the time evolution over the first 30 dynamical times is quite well fitted by two exponentially growing modes, with growth rates in the range  $0.07 \leq \gamma \leq 0.11$  and both modes rotate slowly enough to possess ILRs, although the precision of our frequency estimates is limited by the brevity of the period of linear growth. This contrasts with the original run, shown by the red curve, where many frequencies are present in the evolution to  $t = 40$  that appear to be mostly responses to swing-amplified shot noise.

Not only does this result show that the prior evolution has altered the phase space structure in such a way as to provoke instability, but the growing disturbances owe nothing to pre-existing density variations in the disk, since they were all destroyed by randomizing the azimuths of all the particles. It is therefore inconsistent with other possible explanations for the continued activity that invoke non-linear effects (D’Onghia *et al.* 2013) or mode coupling (Tagger *et al.* 1987; Fuchs *et al.* 2005).

The cyan curve does not rise as rapidly as do the blue and green curves because it was restarted at  $t = 120$  in the original model when the disk had heated somewhat, especially in the inner parts. The vigor of instabilities in the inner disk at later times will be reduced by the increased random motion, while those farther out in the disk would grow more slowly anyway because the dynam-



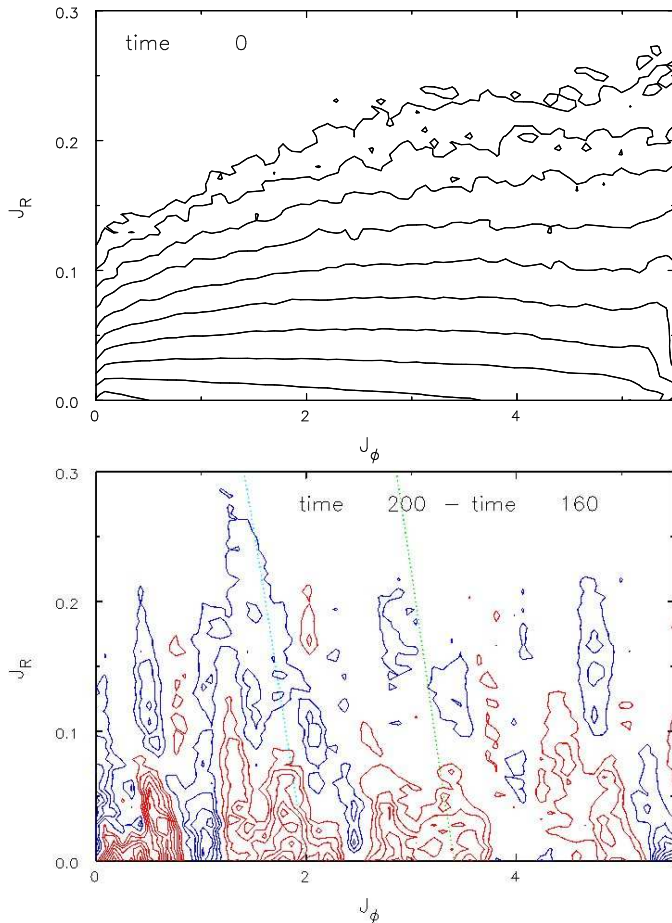


FIG. 8.— Upper panel: the density of particles in the space of the actions ( $J_\phi, J_R$ ) at  $t = 0$  in the  $N = 2 \times 10^6$  particle experiment. The density maximum is near the origin, and the contour spacing is logarithmic; the third contour is at 0.1 and the seventh is at  $10^{-3}$  of the maximum. Lower panel: changes to the density of particles on the same axes between times 160 and 200 in same simulation. Contours in this panel are linearly spaced, and are colored blue where the density has increased, red where the density decreased. The dotted lines indicate the slopes of ILRs in this plane for arbitrarily chosen frequencies; green is for  $m = 3$  and cyan for  $m = 4$ .

ical time scale is longer.

### 3.4. Limiting Amplitude

A mode that grows exponentially at small amplitude must saturate as the second- and higher-order terms, which are neglected in linear analyses, become important. The equilibrium state is unchanged to first order, but it can be altered by the higher-order terms.

During the period when linear theory is adequate, the deflections of the stellar motions caused by the growing potential perturbation must reinforce the perturbed density, else the mode would not grow. However, the orbital deflections of the particles change at finite amplitude; in particular, horseshoe orbits appear near corotation. Sellwood & Binney (2002) argued that the maximum amplitude of a spiral is limited by the widening horseshoe region where stars are driven away from, instead of toward, the density maximum. This change kicks in suddenly because the exponentially growing disturbance density is linearly dependent upon in the disturbance potential, but the width

of the horseshoe region grows as its square-root (Sellwood & Binney 2002). Empirically, the relative overdensity in the disturbance reaches some 20% or 30% before this behavior terminates growth of a linear mode. The wave then begins to decay about as rapidly as it grew (Sellwood & Binney 2002), and all the wave action, *i.e.* angular momentum, stored in the disturbance (Lynden-Bell & Kalnajs 1972) is carried away from corotation at the group velocity (Toomre 1969).

### 3.5. Recurrent Cycle

Once the distribution function, hereafter DF, has become sufficiently non-smooth to provoke one instability, further instabilities can give rise to later spirals. Each is a cavity mode with reflections off corotation, where it is amplified, and some inner radius where recent disturbances have caused abrupt changes to the impedance of the disk.

Evidence for this picture is presented in Fig. 8. The upper panel shows the density of particles in the space of the actions at time 0, while the lower panel shows the change in the density of particles between times 160 and 200 in the same space. The azimuthal action,  $J_\phi \equiv L_z$  in an axisymmetric potential, while the radial action,  $J_R$ , is a measure of the amount of in-and-out motion of the particle. At the initial moment, the density of particles in this space is quite smooth, declining steeply with increasing random motion, and slowly with increasing angular momentum. The differences at later times reveal rising features with steep negative slopes marked by the blue contours that indicate movement of particles to higher  $J_R$  and slightly lower  $J_\phi$ , which is characteristic of ILR scattering. The dotted lines, which have similar slopes to each other and to the ridges, indicate the slopes of two fiducial ILRs for arbitrarily chosen pattern speeds.

The increases in  $J_R$  over this short time period are localized at a small number of ILRs. The consequent abrupt changes to the impedance of the disk cause traveling waves to be sufficiently strongly reflected that the system can support fresh standing waves that are amplified at corotation. As reflections at impedance changes are partial, some wave action continues to the ILR of the mode, where further resonant scattering occurs. Over time, the generally rising level of random motion makes the disk less able to support and amplify coherent waves and activity eventually dies away – unless some cooling is applied.

## 4. OTHER RECENT WORK

Grand *et al.* (2012a,b), Baba *et al.* (2013), and Roca-Fàbrega *et al.* (2013) presented a view of the behavior of spirals in their simulations that differs from ours in at least two substantial respects. We do not question their simulation results, which are consistent with most other work, but we take issue with their interpretation.

### 4.1. Superposed Modes

First, these authors argued that the spirals in their simulations of generally rather low-mass disks appeared to shear continuously. In particular, they almost corotated with the stars at all radii, making them qualitatively different from the usual density wave assumption (*e.g.* Binney & Tremaine 2008).

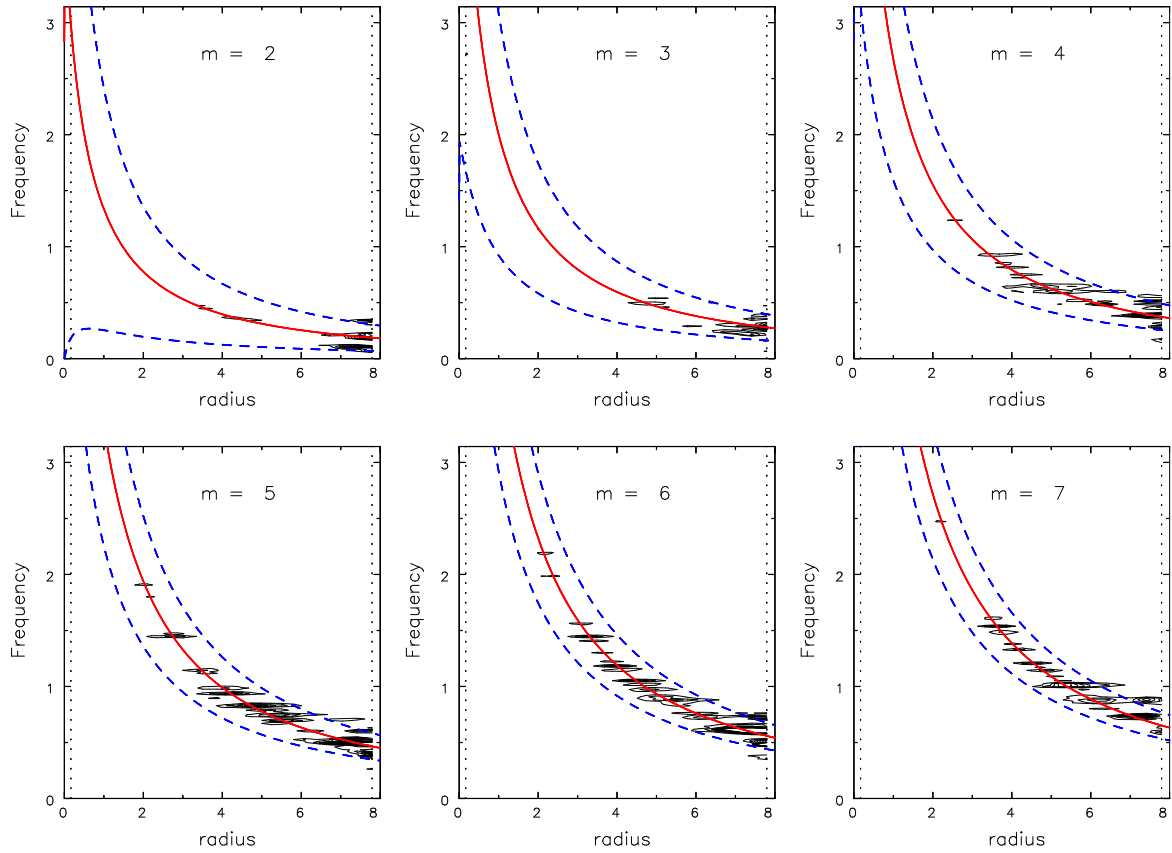


FIG. 9.— Power spectra from the full duration of the low-mass disk model ( $f = 0.2$ ). Notice that there is little power in this model at  $2 \leq m \leq 3$  and most power is for  $m \geq 4$ , whereas sectoral harmonics  $m > 4$ , not shown in Fig. 5, had very little power in the disk with  $f = 0.4$ .

We have run simulations with  $N = 2 \times 10^6$  particles and half the disk mass of those presented above, *i.e.* with  $f = 0.2$ , and observe multi-arm spiral features that appear to shear as these authors describe. However, power spectra, shown in Fig. 9 again reveal coherent waves that qualitatively resemble those in the more massive disk.

Most spiral activity in this low-mass disk occurs with  $m \geq 4$  and there is little power for sectoral harmonics  $m \leq 3$ . Furthermore, waves with higher angular periodicities have smaller radial extents because the Lindblad resonances lie closer to corotation. Higher multiplicity spiral patterns are preferred in lower-mass disks for reasons that are well understood (Paper I). The yardstick for dynamical instabilities,

$$\lambda_{\text{crit}} = \frac{4\pi^2 G\Sigma}{\kappa^2} \quad (8)$$

(Toomre 1964), decreases with the disk mass (for a fixed rotation curve). Swing amplification is strongest where the wavelength of an  $m$ -armed disturbance around its corotation circle

$$\frac{2\pi R_{\text{CR}}}{m} \sim 2\lambda_{\text{crit}} \quad \text{or} \quad m \sim \frac{R_{\text{CR}}\kappa^2}{4\pi G\Sigma}, \quad (9)$$

(Goldreich & Lynden-Bell 1965; Julian & Toomre 1966; Toomre 1981). Thus lower disk mass fractions, for which  $\lambda_{\text{crit}}$  is shorter, favor higher multiplicity patterns.

Fig. 9 reveals that apparently shearing patterns are simply the result of the superposition of multiple separate

modes. The co-existence of two or more waves rotating at different angular rates necessarily produces a shearing density ridge, provided those waves with lower frequency have peak amplitudes at a larger radii.<sup>4</sup> Because these higher-multiplicity spiral modes have a smaller radial extent than those in the high mass disk, the spectra must be computed from long time periods of evolution with frequent analyses to reveal the underlying modal behavior.

#### 4.2. Radial Mixing

The authors of the papers cited at the start of this section offer a description of the mechanism for radial mixing, which still occurred in their simulations, that differs from the standard view (Sellwood & Binney 2002; Roškar *et al.* 2012; Solway *et al.* 2012) that *requires* stars to move through the pattern, albeit slowly.

In fact, the standard view still holds, as shown in Fig. 10, which plots  $\Delta L_z = L_z(400) - L_z(0)$  versus initial  $L_z(0)$  for the particles in the low mass disk. The  $\Delta L_z$  values display similar angled streakiness to that reported by Sellwood & Binney (2002) and by Solway *et al.* (2012) that results from distinct modes, even though the individual patterns may appear to be shearing.

The angular momentum of a particle on a horseshoe orbit changes substantially; those inside corotation gain enough angular momentum to cross the resonance, while

<sup>4</sup> For an animation showing how this is possible, see <http://www.physics.rutgers.edu/~sellwood/spirals.html>.

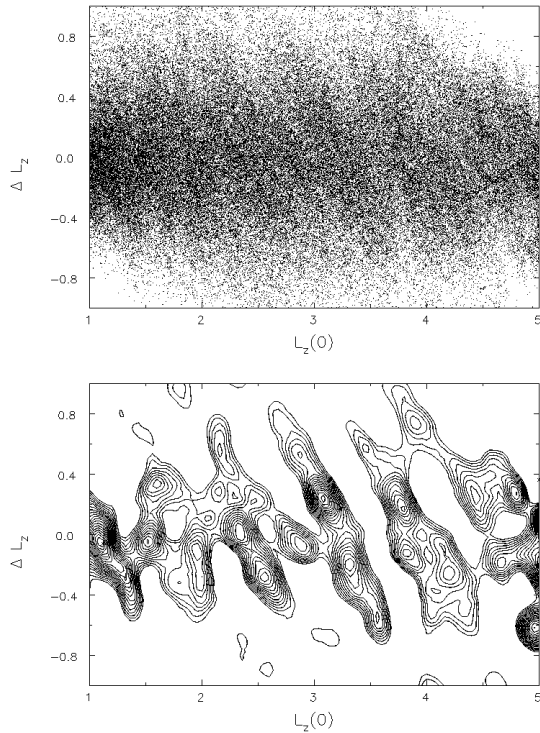


FIG. 10.— Change in angular momentum,  $\Delta L_z$ , vs. initial angular momentum,  $L_z$  for particles in the low-mass disk simulation. The upper panel shows a representative fraction of the particles while the lower panel shows contours of higher than average density in the same plane.

those outside lose a similar amount. The particles experience these changes once only for each transient spiral mode because the disturbance has a large amplitude for less than half a horseshoe orbit period (Sellwood & Binney 2002). Thus the dominant changes to the angular momenta of particles near corotation of a single wave are for low angular momentum particles to gain and high angular momentum particles to lose, giving rise to a single angled streak in this plot. The multiple streaks visible in Fig. 10 arose from multiple coherent waves that each scattered particles across its own corotation resonance, which requires the wave to have had a coherent frequency and to have saturated as described in §3.4.

It should be noted that where linear perturbation theory holds, *i.e.* for small amplitude disturbances away from resonances, the response of the disk particles when multiple waves are present can be computed separately for each wave (see *e.g.* Binney & Tremaine 2008, pp 188-190), with the net response being the sum of the separate linear responses. Thus resonant scattering by one wave is unaffected by the co-existence of other waves, unless resonances were to overlap.

#### 4.3. Slower Disk Heating

Fujii *et al.* (2011), and the authors of the papers cited at the beginning of this section, also reported that spirals heat the disk more slowly than the rate reported in Paper I. Fig. 11 shows that the heating rate is indeed lower in disks with smaller active mass fractions. The reason for the difference is clear: lower-mass disks support pat-

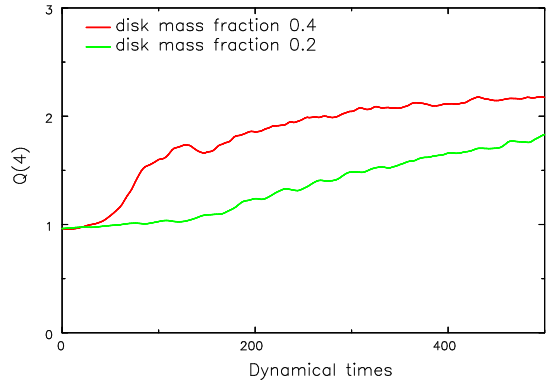


FIG. 11.— Time evolution of  $Q$  at  $R = 4$  in two 3D models with the same  $N = 2 \times 10^6$ , but different active mass fractions. The lighter disk (green) has  $f = 0.2$ , which is half the mass fraction of those shown in Fig. 4, and reproduced in red.

terns of higher multiplicity (Fig. 9), which therefore have Lindblad resonances closer to corotation. Thus the angular momentum transferred outward over the shorter radial extent of these multi-arm patterns releases less energy into non-circular motion (see Fig. 2).

#### 4.4. Heavy Particles

D’Onghia *et al.* (2013) employed  $N = 10^8$  particles in their simulations of a low-mass disk, and experimented with the consequences of adding a few co-orbiting, heavy particles. They ran a model with no heavy particles for about 2.5 disk rotations during which no visible change occurred, but it is likely that non-axisymmetric disturbances were growing that would have appeared had they continued the evolution. (We note that our experiment with a low-mass disk employing merely  $2 \times 10^6$  particles manifested no visible activity, and little heating for perhaps eight rotations, as shown by the green curve in Fig. 11.)

D’Onghia *et al.* (2013) showed that starting similar models with a sprinkling of heavy particles provoked almost immediate multi-armed spiral activity. In one case, they introduced a single perturbing particle that produced a one-armed spiral response and then removed it again one full disk rotation after the start. Four disk rotations after the perturber was removed, they showed that the disk continued to manifest multiple spiral arms, which they attributed to the non-linear evolution of the original disturbance. We suggest instead that their system developed self-excited instabilities due to changes to the originally smooth DF of the disk. Instabilities, which grew out of the initial noise in our experiments were, in their experiment, seeded by the response to the massive co-orbiting particle they introduced, enabling visible self-excited activity immediately thereafter.

Of course, the heavy particles employed by D’Onghia *et al.* (2013) were intended to mimic the molecular cloud complexes possessed by real galaxy disks. Julian & Toomre (1966) showed that a massive, co-orbiting perturber provoked a spiral response in the surrounding stellar disk having an amplitude that scaled with the mass of the perturber. We have preferred to avoid further complicating the dynamical picture with this added realism, as we wish to understand how purely collisionless disks can develop

and support recurring spiral patterns. However, if spirals can develop as self-excited instabilities, as we have argued here, then the role of heavy clumps in the disk is probably not fundamental to the origin of spiral patterns (*cf.* Toomre 1990).

## 5. CONCLUSIONS

We have presented evidence that spiral activity in simulations of cool, unbarred, collisionless stellar disks results from a recurrent cycle of transient spiral modes of spiral form (Fig. 6). We describe them as modes because they start as linear instabilities that grow exponentially even from very low-amplitude (Fig. 7) before saturating and decaying.

Growing modes are standing wave oscillations that have positive feedback to cause instability. We argue that the growing wave train reflects off corotation, where it is swing-amplified, and again at some inner radius, where the distribution function has been modified by previous disturbances in the disk. Scattering of particles at resonances causes localized heating over a moderately narrow range of angular momenta (Fig. 8), which introduces abrupt changes to the impedance experienced by traveling waves. Such changes cause partial reflection of a subsequent wave, allowing a standing wave, or unstable mode to develop.

Spiral instabilities saturate as a result of the onset of horseshoe orbits that appear as the relative overdensity near corotation approaches  $\sim 20\%$ , as originally proposed by Sellwood & Binney (2002). Once growth is halted by the dispersal of the overdensity at corotation, the wave action stored in the remaining disturbance propagates away from corotation until it is absorbed by wave-particle interactions that cause further localized heating. Thus, the instability cycle is able to repeat.

The repeated scattering of particles at different locations leads to a general rise of random motion over the disk that weakens its ability to support further coherent waves, and activity gradually fades on a time-scale of some twenty disk rotations. We have also shown that this timescale is longer in low-mass disks because the multi-arm patterns that are dynamically favored in this case transport angular momentum over a shorter radial distance and, therefore, release less energy into random motions (§4.3).

While we recognize that we have not substantiated all the details, we have presented considerable evidence to support our broad picture. In particular, we find the apparent rapidly changing spirals result from the superposition of a small number of relatively long-lived coherent waves (Fig. 5); the phase coherence and large limiting amplitude of these waves are most naturally accounted for by unstable modes. The evolution of each disturbance creates the seeds for a fresh instability, since we find more vigorous growth in simulations that are restarted after scrambling only the azimuthal phases of the particles (Fig. 7). Not only does this result support our picture, but it shows that the activity in the simulations owes nothing to pre-existing density structures, that were erased by scrambling. Fig. 8 presents evidence of resonance scattering, which we argue changes the impedance of the disk to traveling waves, thereby creating features that cause partial reflection of the waves, allowing fresh cavity modes to develop.

Much of our picture builds on previous work by many

authors: the dispersion relation for spiral waves (Lin & Shu 1966), their group velocity (Toomre 1969), swing-amplification (Goldreich & Lynden-Bell 1965; Julian & Toomre 1966; Toomre 1981), resonance scattering (Lynden-Bell & Kalnajs 1972; Mark 1974), feedback loops (Mark 1977; Toomre 1981), global mode analyses (Zang 1978; Kalnajs 1977; Evans & Read 1998), and horseshoe orbits at corotation (Sellwood & Binney 2002). We could not have reached our present level of understanding without all of these contributions, yet our picture is distinct from any previous suggestion. In particular, we argue that the assumption of a smooth distribution function, which many authors regard as the natural starting point, fundamentally discards the spiral baby with the bathwater!

Direct observational tests of the generating mechanism for spirals are difficult to devise. Evidence for density waves was summarized in the introduction, but does not help to distinguish between rival theories for their origin. However, analysis of the complete phase-space information for a sample of solar neighborhood stars (Sellwood 2010) revealed evidence for a resonant scattering feature, of the kind illustrated in Fig. 8, which supports the picture we present here. Furthermore, the existence of such a feature is inconsistent with other leading theories for the origin of spiral patterns (*e.g.* Bertin *et al.* 1989; Toomre 1990).

## ACKNOWLEDGMENTS

We thank the anonymous referee for a helpful report. This work was supported by NSF grant AST-1108977 to J. A. S., and hospitality from APCTP during the 7th Korean Astrophysics Workshop is gratefully acknowledged. R. G. C. thanks the Canadian NSERC and the Canadian Institute for Advanced Research for support.

## REFERENCES

- Agertz, O., Teyssier, R. & Moore, B. 2011, MNRAS, **410**, 1391  
 Baba, J., Saitoh, T. R. & Wada, K. 2013, ApJ, **763**, 46  
 Belokurov, V., Zucker, D. B., Evans, N. W., *et al.* 2006, ApJL, **642**, L137  
 Bertin, G., Lin, C. C., Lowe, S. A. & Thurstans, R. P. 1989, ApJ, **338**, 78  
 Binney, J. & Tremaine, S. 2008, *Galactic Dynamics* (2nd ed.; Princeton: Princeton University Press)  
 Boylan-Kolchin, M., Springel, V., White, S. D. M. & Jenkins, A. 2010, MNRAS, **406**, 896  
 Carlberg, R. G. & Freedman, W. L. 1985, ApJ, **298**, 486  
 Carlberg, R. G. & Sellwood, J. A. 1985, ApJ, **292**, 79  
 Chemin, L., Balkowski, C., Cayatte, V., *et al.* 2006, MNRAS, **366**, 812  
 Davis, B. L., Berrier, J. C., Shields, D. W., *et al.* 2012, ApJS, **199**, 33  
 D’Onghia, E., Vogelsberger, M. & Hernquist, L. 2013, ApJ, **766**, 34  
 Dubinski, J., Gauthier, J.-R., Widrow, L. & Nickerson, S. 2008, in ASP Conf. Ser. **396** *Formation and Evolution of Galaxy Disks*, ed. J. G. Funes SJ & E. M. Corsini (San Francisco, CA: ASP), 321  
 Evans, N. W. & Read, J. C. A. 1998, MNRAS, **300**, 106  
 French, A. P. 1971, *Vibrations and Waves* (New York: Norton)  
 Fuchs, B., Dettbarn, C. & Tsuchiya, T. 2005, A&A, **444**, 1  
 Fujii, M. S., Baba, J., Saitoh, T. R., *et al.* 2011, ApJ, **730**, 109  
 Gao, L., Frenk, C. S., Boylan-Kolchin, M., *et al.* 2011, MNRAS, **410**, 2309  
 Gnedin, O. Y., Goodman, J. & Frei, Z. 1995, AJ, **110**, 1105  
 Goldreich, P. & Lynden-Bell, D. 1965, MNRAS, **130**, 125  
 Grand, R. J. J., Kawata, D. & Cropper, M. 2012a, MNRAS, **421**, 1529  
 Grand, R. J. J., Kawata, D. & Cropper, M. 2012b, MNRAS, **426**, 167  
 Grosbøl, P., Patsis, P. A. & Pompei, E. 2004, A&A, **423**, 849

- Hockney, R. W. & Brownrigg, D. R. K. 1974, *MNRAS*, **167**, 351
- Inagaki, S., Nishida, M. T. & Sellwood, J. A. 1984, *MNRAS*, **210**, 589
- Julian, W. H. & Toomre, A. 1966, *ApJ*, **146**, 810
- Kalnajs, A. J. 1977, *ApJ*, **212**, 637
- Kendall, S., Kennicutt, R. C. & Clarke, C. 2011, *MNRAS*, **414**, 538
- Kormendy, J. & Norman, C. A. 1979, *ApJ*, **233**, 539
- Lin, C. C. & Shu, F. H. 1966, *PNAS*, **55**, 229
- Lynden-Bell, D. & Kalnajs, A. J. 1972, *MNRAS*, **157**, 1
- Mark, J. W.-K. 1974, *ApJ*, **193**, 539
- Mark, J. W.-K. 1977, *ApJ*, **212**, 645
- Monaghan, J. & Lattanzio, J. 1985, *A&A*, **149**, 135
- Oort, J. H. 1962, in *Interstellar Matter in Galaxies*, ed. L. Woltjer (New York: Benjamin), 234
- Papaloizou, J. C. B. & Lin, D. N. C. 1989, *ApJ*, **344**, 645
- Purcell, C. W., Bullock, J. S., Tollerud, E. J., *et al.* 2011, *Natur*, **477**, 301
- Roca-Fàbrega, S., Valenzuela, O., Figueras, F., *et al.* 2013, *MNRAS*, **432**, 2878
- Roškar, R., Debattista, V. P., Quinn, T. R. & Wadsley, J. 2012, *MNRAS*, **426**, 2089
- Roškar, R., Debattista, V. P., Stinson, G. S., *et al.* 2008, *ApJL*, **675**, L65
- Rybicki, G. B. 1972, in *IAU Colloq. 10, Gravitational N-body Problem*, ed. M. Lecar (Dordrecht: Reidel), 22
- Schweizer, F. 1976, *ApJS*, **31**, 313
- Sellwood, J. A. 1989, in *Dynamics of Astrophysical Discs*, ed. J. A. Sellwood (Cambridge: Cambridge Univ. Press) 155
- Sellwood, J. A. 2010, *MNRAS*, **409**, 145
- Sellwood, J. A. 2011, *MNRAS*, **410**, 1637
- Sellwood, J. A. 2012, *ApJ*, **751**, 44
- Sellwood, J. A. 2013a, in *Planets Stars and Stellar Systems*, v.5, eds. T. Oswalt & G. Gilmore (Heidelberg: Springer), 923 (arXiv:1006.4855)
- Sellwood, J. A. 2013b, *ApJL*, **769**, L24
- Sellwood, J. A. & Athanassoula, E. 1986, *MNRAS*, **221**, 195
- Sellwood, J. A. & Binney, J. J. 2002, *MNRAS*, **336**, 785
- Sellwood, J. A. & Carlberg, R. G. 1984, *ApJ*, **282**, 61
- Shetty, R., Vogel, S. N., Ostriker, E. C. & Teuben, P. J. 2007, *ApJ*, **665**, 1138
- Solway, M., Sellwood, J. A. & Schönrich, R. 2012, *MNRAS*, **422**, 1363
- Tagger, M., Sygnet, J. F., Athanassoula, E. & Pellat, R. 1987, *ApJL*, **318**, L43
- Toomre, A. 1964, *ApJ*, **139**, 1217
- Toomre, A. 1969, *ApJ*, **158**, 899
- Toomre, A. 1981, in *The Structure and Evolution of Normal Galaxies*, ed. S. M. Fall & D. Lynden-Bell (Cambridge: Cambridge Univ. Press), 111
- Toomre, A. 1990, in *Dynamics & Interactions of Galaxies*, ed. R. Wielen (Berlin: Springer), 292
- Tremaine, S. & Weinberg, M. D. 1984, *MNRAS*, **209**, 729
- Visser, H. C. D. 1978, *PhD thesis*, Univ. Groningen
- Zang, T. A. 1976, *PhD thesis*, MIT
- Zibetti, S., Charlot, S. & Rix, H.-W. 2009, *MNRAS*, **400**, 1181